Indium Reduction in Bifacial Silicon Heterojunction Solar Cells with MoO$_x$ Hole Collector

Cao, Liqi; Zhao, Yifeng; Procel Moya, Paul; Han, Can; Kovačević, Katarina; Özkol, Engin; Zeman, Miro; Mazzarella, Luana; Isabella, Olindo

Important note
To cite this publication, please use the final published version (if applicable).
Please check the document version above.

RESEARCH ARTICLE

ADVANCED
ENERGY & SUSTAINABILITY
RESEARCH
Open Access

www.advenergysustres.com

Indium Reduction in Bifacial Silicon Heterojunction Solar Cells with MoO$_x$ Hole Collector

Liqi Cao,* Yifeng Zhao, Paul Procel Moya, Can Han, Katarina Kovačević, Engin Özkol, Miro Zeman, Luana Mazzarella, and Olindo Isabella

Reducing indium consumption in transparent conductive oxide (TCO) layers is crucial for mass production of silicon heterojunction (SHJ) solar cells. In this contribution, optical simulation-assisted design and optimization of SHJ solar cells featuring MoO$_x$ hole collectors with ultra-thin TCO layers is performed. Firstly, bifacial SHJ solar cells with MoO$_x$ as the hole transport layer (HTL) and three types of *n*-contact as electron transport layer (ETL) are fabricated with 50 nm thick ITO on both sides. It is found that bilayer (nc-Si:H/a-Si:H) and trilayer (nc-SiO$_x$:H/nc-Si:H/a-Si:H) as *n*-contacts performed electronically and optically better than monolayer (a-Si:H) in bifacial SHJ cells, respectively. Then, as suggested by optical simulations, the same stack of tungsten-doped indium oxide (IWO) and optimized MgF$_2$ layers are applied on both sides of front/back-contacted SHJ solar cells. Devices endowed with 10 nm thick IWO and bilayer *n*-contact exhibit a certified efficiency of 21.66% and 20.66% when measured from MoO$_x$ and *n*-contact side, respectively. Specifically, when illuminating from the MoO$_x$ side, the short-circuit current density and the fill factor remain well above 40 mA cm^{-2} and 77%, respectively. Compared to standard front/rear TCO thicknesses (75 nm/150 nm) deployed in monofacial SHJ solar cells, this represents over 90% TCO reduction. As for bifacial cells featuring 50 nm thick IWO layers, a champion device with a bilayer *n*-contact as ETL is obtained, which exhibits certified conversion efficiency of 23.25% and 22.75% when characterized from the MoO$_x$ side and the *n*-layer side, respectively, with a bifaciality factor of 0.98. In general, by utilizing a *n*-type bilayer stack, bifaciality factor is above 0.96 and it can be further enhanced up to 0.99 by switching to a *n*-type trilayer stack. Again, compared to the aforementioned standard front/rear TCO thicknesses, this translates to a TCO reduction of more than 67%.

1. Introduction

Front/back-contacted (FBC) silicon heterojunction (SHJ) solar cells have achieved a remarkable conversion efficiency of 26.81%.[1] However, the use of critical raw materials such as indium, silver, and bismuth represents a challenge to realize mass production of SHJ solar cells at the multi-terawatt scale.[2] Especially, the sustainable production capacity of SHJ solar cells is limited to only 37 GW due to the scarcity of indium supply.[2] Therefore, mitigating or minimizing the utilization of indium in SHJ solar cells is crucial to ensure their sustainability for mass production.

Conventionally, the front/rear thickness of transparent conductive oxide (TCO) layers in SHJ solar cells is between 75 and 150 nm, respectively.[3] A TCO layer provides both lateral and vertical transport for charge carriers and protects the underlying layers from metal contact. From an optical point of view, TCO ensures light in-coupling for its thickness-tunable anti-reflective effect. Furthermore, TCO works as a barrier layer against copper diffusion when applying copper plating as the metallization method.[4]

As reported in the literature, there are three main strategies to reduce In consumption. The most straightforward

L. Cao, Y. Zhao, P. Procel Moya, K. Kovačević, E. Özkol, M. Zeman, L. Mazzarella, O. Isabella
Photovoltaic Materials and Devices Group
Delft University of Technology
Delft 2600 AA, The Netherlands
E-mail: L.Cao-3@tudelft.nl

C. Han
School of Materials
Sun Yat-Sen University
No. 135, Xingang Xi Road, Shenzhen 510275, China

solution is to utilize In-free TCOs, such as aluminum-doped zinc oxide (AZO).[5–7] However, more efforts are required to reduce the degradation of fill factor (FF) and to improve the stability of AZO films.[8–10] A second approach is to develop TCO-free SHJ solar cells.[11,12] However, the passivation degrades during metallization process due to the lack of a buffer layer. Besides, as the TCO layer contributes to charge transport, the carrier collection efficiency will decrease in the absence of a TCO. Both passivation degradation and carrier collection require more research effort to fully optimize this structure.[13] Researchers have worked on minimizing the passivation loss induced by metallization process through the utilization of a rather thick doped silicon-based layer. However, this approach resulted in significant parasitic absorption losses.[11] Instead of completely removing the TCO layers, a third solution is to reduce the thickness of TCO layers as compared to typically used TCO thicknesses.[14] Notably, simply reducing the thickness of the TCO layer, which also serves as the anti-reflection coating (ARC) and rear reflector in monofacial SHJ solar cells, will result in increased optical losses in SHJ solar cells. To maintain the good optical response of the solar cells, thinner-than-standard TCOs on the illuminated side are to be combined with an additional transparent layer (e.g., magnesium fluoride, MgF_2), forming a double-layer anti-reflection coating (DLARC). The use of DLARC would significantly reduce reflection losses and improve the current density of the solar cells.[15,16] Moreover, by inserting a dielectric layer between the TCO and the metal electrode on the rear side, an efficient back reflector can be also formed.[17] This is beneficial when reducing the TCO thickness on the rear side of monofacial SHJ solar cells. In the case of TCO reduction in bifacial SHJ solar cells, the use of DLARCs on both sides of the SHJ solar cells is essential to maintain good optical response of solar cells.[14–16,18]

Moreover, it was reported that TCO reduction can be more effectively realized in bifacial SHJ solar cells as compared to monofacial SHJ solar cells,[14,15] as the thickness of both front and rear TCO layers can be decreased to at least 50 nm. So, it will reduce the TCO consumption by 67%. Remarkably, bifacial solar cells could achieve higher annual energy yield compared to monofacial devices,[19] benefitting from the property that light can be absorbed from both sides of the cells. Therefore, in order to achieve better-performing bifacial solar cells, the optical response of the window layers on both sides of the solar cell need to be considered. To achieve both high transparency and conductivity simultaneously, materials such as transition metal oxides (TMO) could be one of the options.[12] For example, MoO_x exhibits higher transparency than silicon-based doped layers[20] and has proven to be an efficient hole transport layer (HTL) in monofacial SHJ solar cells.[21] Therefore, MoO_x can be used at the front side in bifacial SHJ cells. Besides, it is also important to minimize parasitic absorption losses originating from the rear sides of the cells. Silicon-based materials such as doped hydrogenated nanocrystalline silicon (nc-Si:H) and its alloyed version with oxygen (nc-SiO$_x$:H) are preferred as the electron transport layer (ETL) on the rear side of SHJ solar cells as compared to typically used (n)a-Si:H.[3,22–27]

Aiming at reducing indium consumption, we explore the possibility of lowering the thickness of indium-based TCO layer while avoiding degradation in cell performance. First, we evaluate the performance of bifacial SHJ solar cells featuring various rear-side n-contact, namely, monolayer (a-Si:H), bilayer (nc-Si:H/a-Si:H), and trilayer (nc-SiO$_x$:H/nc-Si:H/a-Si:H), combined with MoO_x at the front side. Then, the optical and electrical properties of thin-film IWO deposited on glass substrates with varied thicknesses from 10 nm to 50 nm are assessed. Subsequently, optical simulations are carried out to investigate the optical potential of bifacial SHJ solar cells utilizing ultra-thin IWO films in combination with MgF_2 films to form DLARCs. Eventually, bifacial SHJ solar cells with ultra-thin IWO films are manufactured and analyzed.

2. Results and Discussion

2.1. The Influence of Different *n*-Type Layers on Cell Performance

We first investigated the performance of solar cells fabricated with three different n-contact depicted in **Figure 1**A, consisting of i) a monolayer (a-Si:H), ii) a bilayer (nc-Si:H/a-Si:H) or iii) a trilayer (nc-SiO$_x$:H/nc-Si:H/a-Si:H). At this initial stage, we applied 50-nm-thick ITO on both sides of bifacial FBC-SHJ solar cells. The external parameters are reported in Figure 1B. We measured the solar cells without and with an additional 100-nm-thick MgF_2 to form a DLARC with ITO on both sides of the solar cells. The results obtained by illuminating the solar cells from MoO_x and n-contact are marked as P-side and N-side, respectively. The results are presented in Figure 1B,C.

As depicted in Figure 1B, prior to the application of MgF_2, the open-circuit voltage (V_{OC}) of the solar cells when illuminated from the P-side is quite similar. However, the data measured for illumination from the N-side are different due to different n-type layer stacks. Specifically, the bilayer structure provides a better passivation effect compared to the other two n-contacts.[3] The short-circuit current densities (J_{SC}) measured from the P-side share similar values for bilayer and trilayer samples and are slightly higher than the values measured from monolayer samples. The J_{SC} values measured from N-side are quite different, with the trilayer samples exhibiting the highest J_{SC}, followed by bilayer and monolayer samples. This is attributed to the nc-SiO$_x$:H layer displaying significantly lower parasitic absorption in comparison to nc-Si:H and a-Si:H layers.[3,28] In contrast, the FF values measured from bilayer samples achieved highest value, followed by monolayer and then trilayer samples. This may be attributed to the better electronic properties of the nc-Si:H layer compared to the other two layers.[3]

After applying the additional MgF_2 layers, similar trends on V_{OC} are found for all three n-contacts. Nevertheless, when solar cells were illuminated from the N-side, their FFs were slightly higher compared to those illuminated from P-side within each group. These results demonstrate that the carrier transport property of the N-side is better than the P-side.

To be more specific, as shown in Figure 1B, the bilayer n-type stack exhibits the highest FF among all n-contacts investigated, then followed by the monolayer (n)a-Si:H, and lastly, by the trilayer stack. This is mainly due to the rather thick (≈10 nm) and the less favorable electrical properties of (n)nc-SiO$_x$:H.[3,29] The FF is negligibly influenced by the deposition of MgF_2. There is a noticeable variation in J_{SC} when solar cells were illuminated
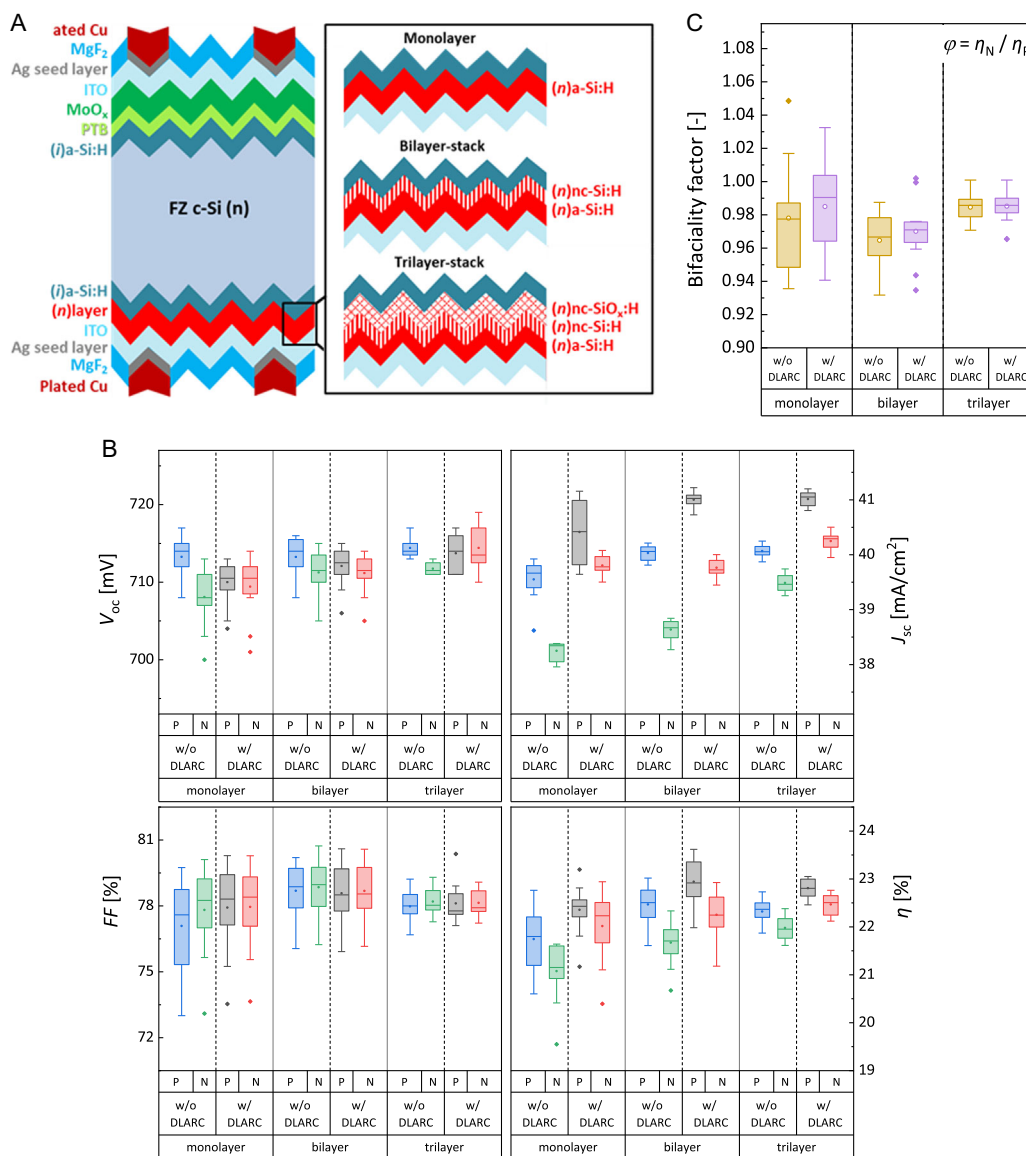
Figure 1. A) Schematic illustration of bifacial SHJ solar cells with three types of n-layer stacks. B) The external parameters of bifacial cells with different n-layer stacks, and C) the bifaciality factors. All the cells are measured by illuminating either the MoO$_x$ or the n-layer side indicated as P and N, respectively. 12 cells with 50 nm thick ITO on both sides are included in each box plot.

from N and P sides within each group. Specifically, the J_{SC} is generally higher when the cells are illuminated from the P side compared to when illuminated from N-side. This can be explained by better transparency of MoO$_x$. When comparing cells with different n-contacts, we note that the trilayer-stack delivers the best light response of solar cells, which exhibits average gains of 0.8 and 1.2 mA cm^{-2} as compared to bilayer-stack and monolayer (n)a-Si:H, respectively.

The bifaciality factor (φ) of the devices is calculated and shown in Figure 1C. Solar cells with monolayer- and trilayer-stack exhibit the best bifaciality factor of 0.99, indicating the capability of realizing higher power generations as compared to monofacial cells. It is noticeable that the φ of few samples featuring monolayer is above 1 which suggests the efficiency measured from

N-side is higher than the P-side. This could be attributed to fluctuations during fabrication and measurement process. While the φ of cells with bilayer-stack is around 0.96, which is mainly caused by higher FF for the P-side illumination and slightly lower J_{SC} for the N-side illumination as compared to the other two types of n-contact. The champion cell with bilayer-stack exhibits a conversion efficiency of 23.62% when measured from the P side ($V_{OC} = 715$ mV, $J_{SC} = 40.98$ mA cm^{-2}, FF = 80.6%) and 22.83% efficiency from the N side ($V_{OC} = 714$ mV, $J_{SC} = 39.67$ mA cm^{-2}, FF = 80.6%). According to our findings, bilayer and trilayer stacks exhibit higher conversion efficiency for the application in bifacial solar cells. Therefore, we will utilize these two n-contact in the following experiments.

2.2. Optical and Electrical Properties of IWO

In comparison to ITO films, IWO films demonstrate better light response due to lower absorption in the wavelength range of interest.[30] As the TCO properties are influenced by the layer's thickness,[31] to eventually implement ultra-thin TCO layers into solar cells, the opto-electrical properties of IWO with different thickness are evaluated. The carrier density (N_e), mobility (μ_e), and resistivity (ρ) of the IWO film exhibit variations as a function of thickness, as illustrated in **Figure 2**. The results show that, the N_e and μ_e increase and the ρ decreases as the IWO thickness increases.

The correlation between a decrease in ρ and an increase in thickness could be elucidated by the crystalline structure of the film. According to a reported research, an increase in film thickness is associated with a growth in the grain size of the IWO, resulting in a decline of electrical resistivity through more effective doping and a reduction in grain boundary scattering.[32,33] Additionally, the enhancement in film crystallinity

that occurs with increased thickness is believed to contribute to an increase in μ_e.[32,34,35]

After the annealing process step, which was required to recover passivation after sputtering in our SHJ cell fabrication process, the mobility of IWO layers improved[36] while the N_e of these films showed slight decrements. For instance, the N_e of 50 nm thick IWO film decreased from 3.0×10^{20} to 2.5×10^{20} cm^{-3}. The N_e decreases after annealing could be caused by oxygen incorporation.[30] In contrast, the μ_e increased after annealing especially for 10 and 20-nm-thick IWO samples. The μ_e of 10 nm thick IWO increases significantly from 29 to 34 cm^2 V^{-1} s^{-1} after annealing. This phenomenon could be explained by that thinner layer is more sensitive to annealing.[37] The improvement may be more significant when annealing the thin IWO films. However, ρ is also increased after annealing. We notice that the ρ of 10 nm thick IWO sample increased from 34×10^{-4} to 62×10^{-4} Ω cm. An increase in ρ and a decrease in N_e will lead to decreased carrier transport efficiency in the device, ultimately affecting FF values.[35,38]
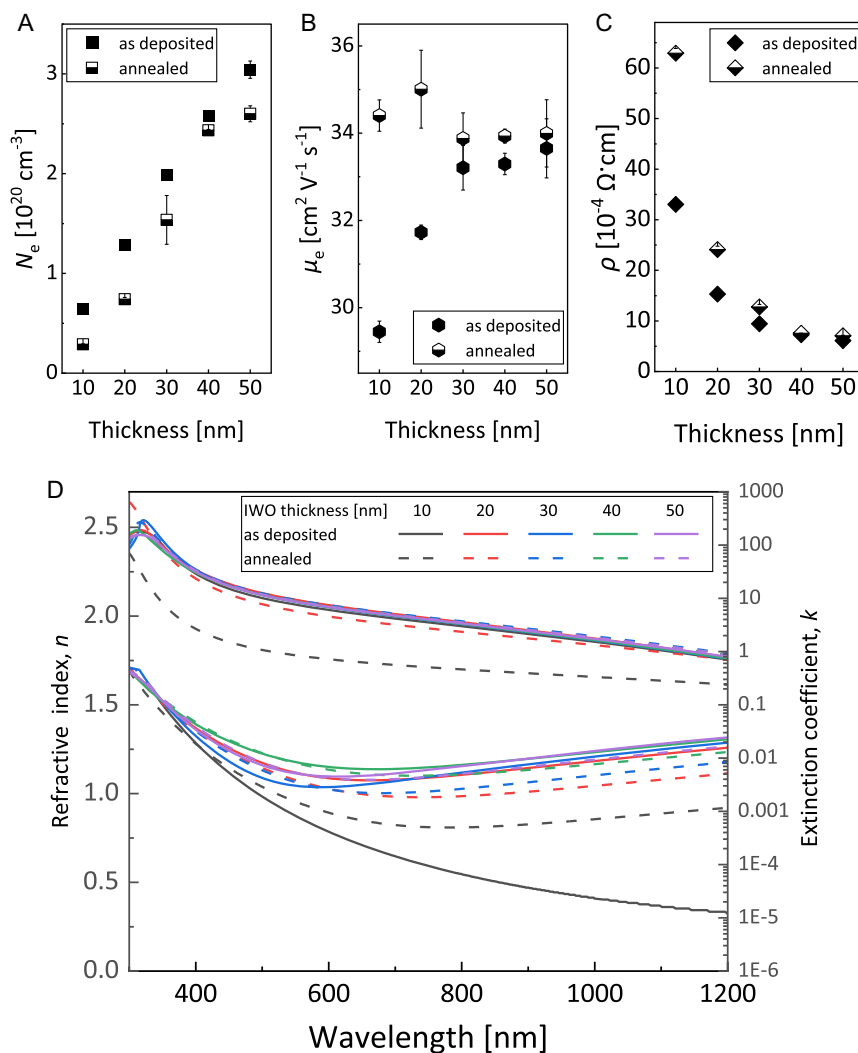

Figure 2. A–C) Carrier density (N_e), mobility (μ_e), and resistivity (ρ) as a function of IWO thickness measured before and after annealing. D) Complex refractive index of IWO layers with different thicknesses (left axis: refractive index; right axis: extinction coefficient).

ADVANCED
SCIENCE NEWS
www.advancedsciencenews.com

ADVANCED
ENERGY & SUSTAINABILITY
RESEARCH
Open Access
www.advenergysustres.com

Furthermore, the electrical properties of the IWO relate to the optical properties. Figure 2D shows the complex refractive index as a function of IWO thickness. The 10 nm thick IWO layer provides the highest transparency in UV range compared to thicker layers. After annealing, the extinction coefficient (k) exhibited an increase from 600 to 1200 nm range. In contrast, the k value of thicker layers decreased after annealing in the same wavelength range. Consequently, annealing led to enhanced transparency in longer wavelength for IWO layers, except for the 10 nm thick sample.

2.3. Optical Simulation Results with Ultra-Thin IWO

To investigate the optical potential of our bifacial SHJ solar cells while reducing the thickness of In-based TCO layers, we performed optical simulations using GenPro4.[39] The simulation results, shown in **Figure 3**, are based on the schematic structure of the bifacial SHJ solar cell in Figure 1A. To reduce the parasitic absorption losses induced by ITO films on both sides of solar cells, optimized IWO layers were used instead.[15] Besides, as already demonstrated in ref. [15], bifacial SHJ solar cells with good electrical performance can be achieved with only 25 nm thick TCO layers when combined with around 100 nm thick SiO_x on both sides, forming DLARC. MgF_2 as an alternative DLARC with lower refractive index comparing to SiO_2, was applied in optical simulation. In the optical simulations, we varied IWO thickness from 10 nm to 50 nm on both sides of the device as well as the MgF_2 layer thickness. The incident light intensities at the P side and N side are 1000 and 200 W cm^{-2}, respectively.[40] The implied photocurrent density of bifacial cells ($J_{\text{implied-bifi}}$) was calculated by summing up the implied photocurrent densities' (J_{implied}) contributions obtained from both sides. To elucidate the increase of J_{implied} ($\Delta J_{\text{implied}}$) from monofacial to bifacial structures, we conducted simulations on implied

photocurrent density of front side ($J_{\text{implied-front}}$) and implied photocurrent density of the bifacial solar cell with 1.0 Sun illumination at the front side and 0.2 Sun illumination at the rear side. Results of that simulation campaign are reported in Figure S1–S3, Supporting Information. The white star in Figure 3 indicates the highest $J_{\text{implied-bifi}}$ and the x and y axis regard the thickness of MgF_2 on the front and rear side, respectively.

As illustrated in Figure 3, the highest $J_{\text{implied-bifi}}$ increases with the increasing of IWO thickness for both bilayer and trilayer types of (n)-contacts. When using 10 nm thick IWO, MgF_2 layers of 110 nm (front) and 120 nm (rear) are needed to maximize the $J_{\text{implied-bifi}}$ of the bifacial solar cells, reaching a value of 47.8 mA cm^{-2} as shown in Figure 3A,B. The lower maximum $J_{\text{implied-bifi}}$ of cells with 10 nm thick IWO as compared to those with 50 nm thick IWO is due to higher reflectance. Measured reflectance of bifacial solar cells is presented in Figure S4, Supporting Information. Based on simulation results, we fabricated solar cells with varying IWO front/rear thickness (10 nm through 50 nm) and correspondingly optimized MgF_2 layers on both sides.

It is noticeable that the thickness of MgF_2 layer on the front side dominates the current contribution to the bifacial device, so thickness of MgF_2 layer on front side should be carefully optimized. As shown in Figure 3, there is much more tolerance in the rear side MgF_2 and IWO use.

2.4. Ultra-Thin IWO Layers for Bifacial Silicon Heterojunction Solar Cells

The external parameters of bifacial solar cells with bilayer n-type stack are reported in **Figure 4**A. The V_{OC} of the cells increases with the increase of IWO thickness. A similar trend is found also for J_{SC}, FF, and η. The TCO in SHJ solar cells works serves a dual purpose. It does not only function as anti-reflection coating for
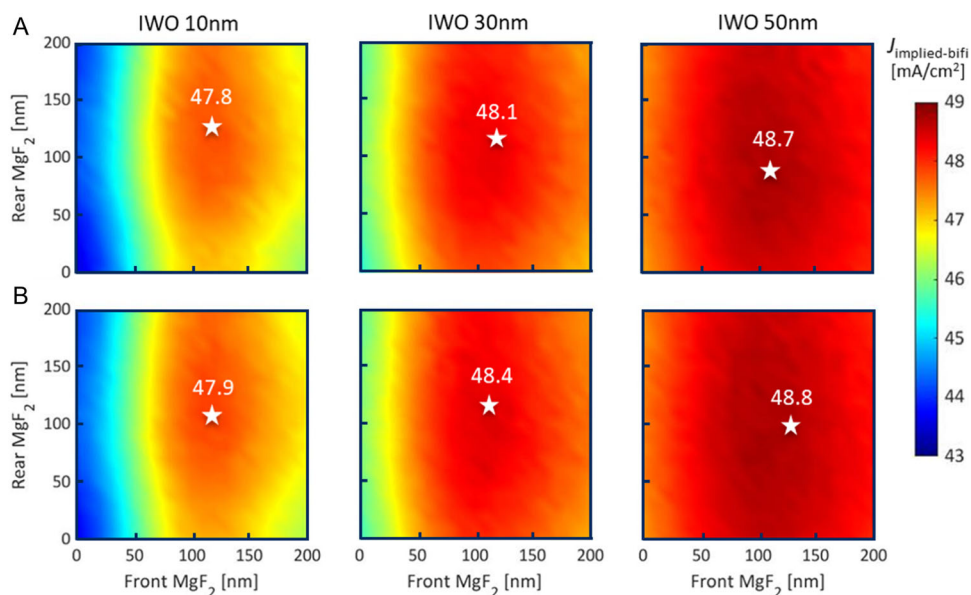

Figure 3. Optical simulation results of bifacial solar cells with A) bilayer n-type stack and B) trilayer n-type stack. The white star represents the optimal combination of MgF_2 thickness on the front and rear side in combination with fixed front/rear IWO thickness.
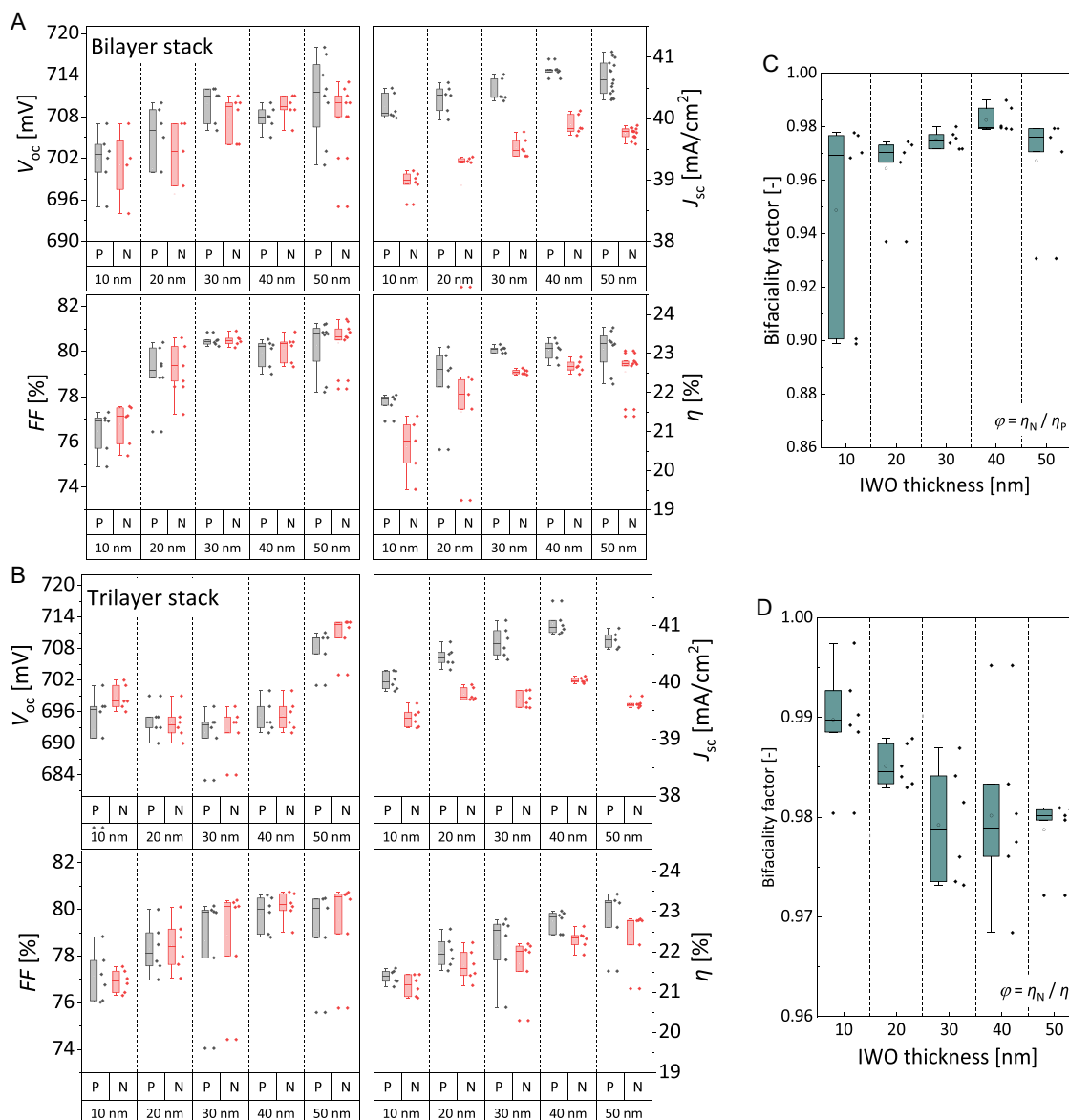
Figure 4. A,B) All cells are measured by illuminating either the MoO$_x$ layer or the n-contact side corresponding to P-side and N-side, respectively (the grey and red bars indicate the data measured from the P-side and the N-side of the bifacial cells, respectively). The conversion efficiencies at N-side and P-side illuminations are used to calculate the bifaciality factor of bifacial cells with C) bilayer or (D) trilayer n-contact.

optical purpose but also facilitates lateral transport for carriers.[8,41] IWO is a n-type material, so it might also provide field effect passivation in solar cells.[42] Consequently, increasing IWO thickness may potentially enhance V_{OC}, J_{SC}, FF, and η. However, the FF measured when illuminating the device through the N-side is slightly higher than the values measured from the P-side, demonstrating once more that the carrier transport property of the N-side is better than that of the P-side.[43] The higher J_{SC} measured from P-side can be attributed to better transparency of MoO$_x$.[21] It is worth noting that the J_{SC} varied with different IWO-thickness, consistently with optical simulation results. Thicker IWO provided better light response.

Nevertheless, a decrease in J_{SC} was observed at 50 nm thick IWO samples. According to the external quantum efficiency (EQE) measurement as shown in Figure S5, Supporting Information, we assume this is due to the insufficient MgF$_2$ thickness on the rear side.

The external parameters of bifacial solar cells with trilayer n-type stack are plotted in Figure 4B. FF and η have the same trends as the case for bilayer stack samples. The resistivity and sheet resistance of IWO across various thicknesses are presented in Figure S6, Supporting Information, where a consistent trend with FF is observed. Consequently, the variations in FF across different IWO thicknesses can be attributed to changes

**ADVANCED
SCIENCE NEWS**

www.advancedsciencenews.com

**ADVANCED
ENERGY & SUSTAINABILITY
RESEARCH**

www.advenergysustres.com

in resistivity and sheet resistance. The lower V_{OC} values measured in this series are most probably caused by different passivation qualities of the cell precursors. The enhancement of V_{OC} in 50 nm case could be ascribed to the higher lifetime of the cell precursor as provided in Figure S7, Supporting Information. The passivation quality of trilayer samples is generally lower than that of the bilayer stack samples. This could be linked to a less conductive n-layer close to the c-Si/(i)a-Si:H interface due to the use of less conductive nc-SiO$_x$:H layer; therefore, field-effect passivation or the band bending is less efficient. The deposition condition of the trilayer is more aggressive compared to that of bilayer and monolayer samples. As in the bilayer-stack case, here we also note a decrease of J_{SC} value for 30 and 50 nm thick IWO, due to the insufficient MgF$_2$ thickness.

When comparing the N-side-J_{SC} between the two n-contact, it was observed that the trilayer-stack had a better light response, showing an average gain of 0.3 mA cm^{-2} as compared to cells with the bilayer-stack. This gain might be attributed to reduced reflected light as shown in Figure S4, Supporting Information. However, as previously mentioned, mainly due to the rather thick stack ($\approx$10 nm) and the less favorable electrical properties of (n)nc-SiO$_x$:H, the samples with trilayer-stack exhibit lower FF as compared to those with bilayer n-type stack.

The optical simulation and experimental results exhibited a strong correlation. The J_{SC} increased with thicker IWO layer. It was observed that even with a thickness of only 10 nm for IWO, a decent J_{SC} can be maintained. However, the FF of the device with 10 nm thick IWO was found to be below 78%, which can be attributed to the high contact resistance as illustrated in Figure 2C and as well as in ref. [31]

The φ of the devices is shown in Figure 4C,D. Solar cells with trilayer n-type stack exhibit the best average bifaciality factor of 0.99, while the bifaciality factor of cells with bilayer n-type stack is around 0.96. This difference was mainly caused by a larger variation in J_{SC} when illuminated from N-side due to the better light response of trilayer stack comparing to bilayer stack. The champion cell with bilayer n-type stack exhibits 23.25% conversion efficiency when measured from the P-side ($V_{OC} = 716$ mV, $J_{SC} = 39.74$ mA cm^{-2}, FF = 81.7%) and 22.75% efficiency from the N-side ($V_{OC} = 716$ mV, $J_{SC} = 38.87$ mA cm^{-2}, FF = 81.9%). **Figure 5** shows the independently certified efficiencies of our best performing solar cell.

3. Conclusion

This study aims to reduce TCO consumption by minimizing TCO thickness in bifacial solar cells while preserving high solar cell performance. Our study investigated the impact of different n-contacts and various thicknesses of IWO films on the performance of bifacial solar cells. We found that bilayer and trilayer stack exhibited higher efficiency compared to monolayer stack mainly due to better i) electronic properties of bilayer stack and ii) optical properties of trilayer stack. The optical simulation demonstrates that the integration of thinner IWO layers into bifacial solar cells combined with bilayer and trilayer stack yields a promising enhancement in light response. Even with only 10 nm thick IWO, the cells achieve J_{SC} over 40 mA cm^{-2}. Additionally, by symmetrically applying IWO and MgF$_2$ layers on both sides of the solar cells and reducing the thickness to 10 nm, we achieved certified conversion efficiencies of 21.66% and 20.66% when measured from the MoO$_x$ and n-contact side, respectively, with J_{SC} and FF values remaining above 40 mA cm^{-2}% and 77%. In this way, a reduction of 90% in the usage of IWO compared to monofacial SHJ solar cells was demonstrated. The certified results are shown in Figure S8, Supporting Information. For 50 nm thick IWO samples, the champion device within a bilayer-stack achieves certified conversion efficiencies of 23.25% and 22.75% when characterized from the MoO$_x$ side and the n-layer side, respectively, with a bifaciality factor of 0.98. In general, a bilayer stack can result in a bifaciality factor above 0.96, which can be further enhanced to 0.99 by switching to a trilayer stack. These findings demonstrate the potential of bilayer and trilayer stack with IWO films as promising candidates for high-performance bifacial solar cells sporting more than 90% reduction in usage of TCO.

4. Experimental Section

Solar Cells with Different n-Type Layers: The samples were prepared using 4 in. double-side-polished n-type float zone (FZ) wafers with <100> orientation. The resistivity and thickness of the wafers were $3 \pm 2 \, \Omega$ cm and $280 \pm 20 \, \mu$m, respectively. The wafer texturing process was conducted in a TMAH solution with ALKA-TEX as an additive.[44] Next, the wafers were cleaned using wet-chemical cleaning and subsequent dipping in 0.55% hydrogen fluoride (HF) for 5 min.[45–47] Afterwards, the wafers were loaded into a multi-chamber plasma-enhanced
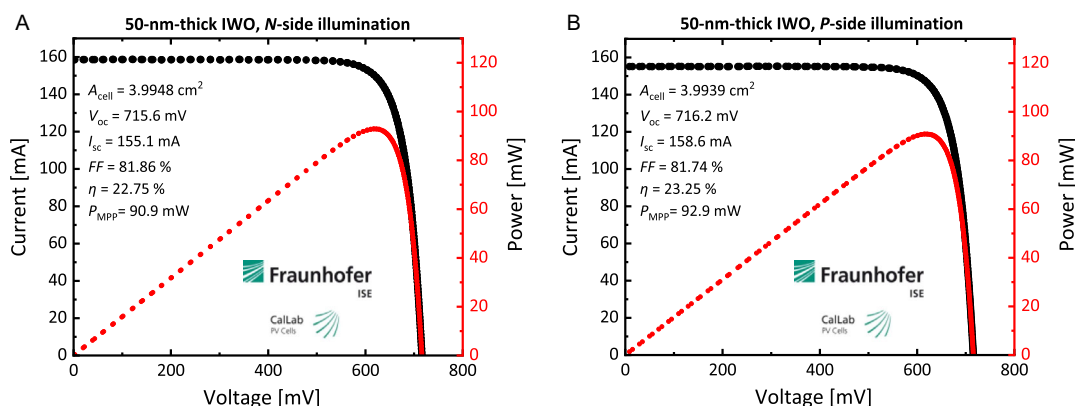

Figure 5. A,B) certified power conversion efficiency for 50 nm IWO cells from N and P side, respectively.

chemical vapor deposition (PECVD) equipment for the deposition of thin-film silicon layers. (*i*)a-Si:H layers were deposited on both sides of the wafers and three different types of electron transport layers (ETL) were deposited at the rear side: i) 4 nm monolayer (*n*)a-Si:H, ii) bilayer with 3 nm (*n*)nc-Si:H/2 nm (*n*)a-Si:H,[3] iii) trilayer with 8 nm (*n*)nc-SiO$_x$:H/3 nm (*n*)nc-Si:H/2 nm (*n*)a-Si:H In.[8,11,12] Subsequently, (*i*)a-Si:H layer was deposited on the front side of the samples. An interface treatment, namely PTB,[21] was introduced during the PECVD process. This treatment involved the utilization of a gas mixture containing SiH$_4$, H$_2$, CO$_2$, and B$_2$H$_6$, which was highly diluted with hydrogen ($\approx$170 sccm). PTB was applied prior to the thermal evaporation of MoO$_x$, more detailed information can be found in our previous work.[21] After that, optimized TCO layers were sputtered through a hard mask at front and rear side, respectively, defining six 2 $\times$ 2 cm^2 solar cells per wafer.[30] The front and rear metal electrode consists of simultaneously electroplated Cu fingers at room temperature on top of 200 nm thick thermally evaporated Ag seed layer.[44,48] The width of the fingers was 15 µm and the pitch between two fingers was 915 µm. Finally, MgF$_2$ films were e-beam evaporated on both sides as additional anti-reflection coating layers.

Deposition of IWO Films: Corning glasses were used as the substrate for the deposition of IWO films; and they were cleaned by isopropyl and acetone in a supersonic bath for 10 min each. IWO films were deposited on cleaned Corning glasses by RF magnetron sputtering technique (Polyteknic AS) at room temperature. Ar was used as the sputtering gas with a flow of 20 sccm (mixed with 0.25% O$_2$). The pressure of the deposition chamber was 4.0×10^{-3} mbar and the power density was around 0.8 W cm^{-2}. The target composition of IWO was 95 wt% In$_2$O$_3$ and 5 wt% WO$_3$. The base pressure of the chamber before deposition is below 1×10^{-7} mbar. The deposition rate was around 2 nm min^{-1} on flat surface. Since the surface of wafer-based substrates was textured, the deposition time is calculated by multiplying a geometrical factor of 1.7 based on the deposition time on the flat surface. To cure the passivation quality damaged by ion bombardment during the sputtering, a post-annealing treatment was performed in an oven with air atmosphere at 180 °C for 5 min. Carrier concentration, Hall mobility, and resistivity of the samples were obtained from Hall Effect measurements.

Characterizations: Effective minority carrier lifetime was measured at different steps of the fabrication flow chart by Sinton WCT-120 equipment. Current-voltage characteristics of solar cells were determined using an AAA-rated Wacom WXS-90S-L2 solar simulator under standard test conditions (STC). A specially designed chuck for bifacial solar cell measurement was in-house design and realized for bifacial solar cell measurements. In this chuck, a specialized substrate was utilized which displayed a reflectance of less than 3.5% across the wavelength range of 700–1200 nm. The substrate's reflectance and transmittance curves have been presented in previous work of our lab.[48] By mounting the wafer directly on this substrate during the *J*–*V* measurements, the influence of rear-side illumination on the front-side measurements was effectively mitigated, with the controlled amount remaining below 3 Wm^{-2}.[19] The *J*–*V* data was obtained separately from both sides of the SHJ devices. In this work, the bifaciality factor (φ) is defined as $\varphi = \eta_N/\eta_P$. η_N is the efficiency measured from the *N*-side and η_P is the efficiency measured from the *P*-side.

Supporting Information

Supporting Information is available from the Wiley Online Library or from the author.

Acknowledgements

Conflict of Interest

The authors declare no conflict of interest.

Data Availability Statement

The data that support the findings of this study are available from the corresponding author upon reasonable request.

Keywords

[1] H. Lin, M. Yang, X. Ru, G. Wang, S. Yin, F. Peng, C. Hong, M. Qu, J. Lu, L. Fang, C. Han, P. Procel, O. Isabella, P. Gao, Z. Li, X. Xu, *Nat. Energy* **2023**, *8*, 789.

[2] Y. Zhang, M. Kim, L. Wang, P. Verlinden, B. Hallam, *Energy Environ. Sci.* **2021**, *14*, 5587.

[3] Y. Zhao, L. Mazzarella, P. Procel, C. Han, F. D. Tichelaar, G. Yang, A. Weeber, M. Zeman, O. Isabella, *Prog. Photovolt. Res. Appl.* **2021**, *30*, 809.

[4] J. Yu, J. Li, Y. Zhao, A. Lambertz, T. Chen, W. Duan, W. Liu, X. Yang, Y. Huang, K. Ding, *Sol. Energy Mater. Sol. Cells* **2021**, *224*, 110993.

[5] Z. Wu, W. Duan, A. Lambertz, D. Qiu, M. Pomaska, Z. Yao, U. Rau, L. Zhang, Z. Liu, K. Ding, *Appl. Surf. Sci.* **2021**, *542*, 148749.

[6] Q. Tang, W. Duan, A. Lambertz, K. Bittkau, M. A. Yaqin, Y. Zhao, K. Zhang, Q. Yang, D. Qiu, F. Gunkel, *Sol. Energy Mater. Sol. Cells* **2023**, *251*, 112120.

[7] A. B. Morales-Vilches, A. Cruz, S. Pingel, S. Neubert, L. Mazzarella, D. Meza, L. Korte, R. Schlatmann, B. Stannowski, *IEEE J. Photovolt.* **2018**, *9*, 34.

[8] A. Cruz, E.-C. Wang, A. B. Morales-Vilches, D. Meza, S. Neubert, B. Szyszka, R. Schlatmann, B. Stannowski, *Sol. Energy Mater. Sol. Cells* **2019**, *195*, 339.

[9] D. Greiner, S. E. Gledhill, C. Köble, J. Krammer, R. Klenk, *Thin Solid Films* **2011**, *520*, 1285.

[10] J. I. Kim, W. Lee, T. Hwang, J. Kim, S.-Y. Lee, S. Kang, H. Choi, S. Hong, H. H. Park, T. Moon, *Sol. Energy Mater. Sol. Cells* **2014**, *122*, 282.

[11] S. Li, M. Pomaska, A. Lambertz, W. Duan, K. Bittkau, D. Qiu, Z. Yao, M. Luysberg, P. Steuter, M. Köhler, K. Qiu, R. Hong, H. Shen, F. Finger, T. Kirchartz, U. Rau, K. Ding, *Joule* **2021**, *5*, 1535.

[12] J. He, G. Wang, Y. Qiu, Z. Tang, F. Ye, C. Zhang, S. Wang, L. Cai, T. Yu, P. Gao, *Adv. Funct. Mater.* **2022**, *32*, 2205901.

[13] P. Wagner, A. Cruz, J. C. Stang, L. Korte, *IEEE J Photovolt* **2021**, *11*, 914.

[14] T. Gageot, J. Veirman, F. Jay, D. Muñoz-Rojas, C. Denis, R. Couderc, A. S. Ozanne, R. Monna, S. Zogbo, R. Cabal, *Sol. Energy Mater. Sol. Cells* **2023**, *261*, 112512.

[15] C. Han, R. Santbergen, M. van Duffelen, P. Procel, Y. Zhao, G. Yang, X. Zhang, M. Zeman, L. Mazzarella, O. Isabella, *Prog. Photovolt. Res. Appl.* **2022**, *30*, 750.

[16] Z. Sun, X. Chen, Y. He, J. Li, J. Wang, H. Yan, Y. Zhang, *Adv. Energy Mater.* **2022**, *2200015*, 2200015.

[17] Z. C. Holman, A. Descoeudres, S. De Wolf, C. Ballif, *IEEE J. Photovolt.* **2013**, *3*, 1243.

**ADVANCED
SCIENCE NEWS**

www.advancedsciencenews.com

**ADVANCED
ENERGY & SUSTAINABILITY
RESEARCH**
Open Access

www.advenergysustres.com

[18] A. Cruz, D. Erfurt, P. Wagner, A. B. Morales-Vilches, F. Ruske, R. Schlatmann, B. Stannowski, *Sol. Energy Mater. Sol. Cells* **2022**, *236*, 111493.

[19] T. S. Liang, M. Pravettoni, C. Deline, J. S. Stein, R. Kopecek, J. P. Singh, W. Luo, Y. Wang, A. G. Aberle, Y. S. Khoo, *Energy Environ. Sci.* **2019**, *12*, 116.

[20] L. Neusel, M. Bivour, M. Hermle, *Energy Procedia* **2017**, *124*, 425.

[21] L. Cao, P. Procel, A. Alcañiz, J. Yan, F. Tichelaar, E. Özkol, Y. Zhao, C. Han, G. Yang, Z. Yao, *Progr. Photovolt. Res. Appl.* **2022**, *31*, 1245.

[22] L. Mazzarella, A. B. Morales-Vilches, M. Hendrichs, S. Kirner, L. Korte, R. Schlatmann, B. Stannowski, *IEEE J. Photovolt.* **2018**, *8*, 70.

[23] L. Mazzarella, A. B. Morales-Vilches, L. Korte, R. Schlatmann, B. Stannoswki, *Sol. Energy Mater. Sol. Cells*, **2018**, *179*, 386.

[24] A. Richter, V. Smirnov, A. Lambertz, K. Nomoto, K. Welter, K. Ding, *Sol. Energy Mater. Sol. Cells* **2018**, *174*, 196.

[25] L. Mazzarella, S. Kirner, B. Stannowski, L. Korte, B. Rech, R. Schlatmann, *Appl. Phys. Lett.* **2015**, *106*, 023902.

[26] X. Ru, M. Qu, J. Wang, T. Ruan, M. Yang, F. Peng, W. Long, K. Zheng, H. Yan, X. Xu, *Sol. Energy Mater. Sol. Cells* **2020**, *215*, 110643.

[27] R. Martins, A. Maçarico, I. Ferreira, R. Nunes, A. Bicho, E. Fortunato, *Thin Solid Films* **1997**, *303*, 47.

[28] Y. Yang, W. Liu, L. Zhang, S. Huang, X. Li, K. Jiang, Z. Li, Z. Yan, S. Lan, X. Wu, Z. Ma, Y. Zhou, Z. Liu, *Mater. Lett.* **2022**, *309*, 131360.

[29] Y. Zhao, L. Mazzarella, P. Procel, C. Han, G. Yang, A. Weeber, M. Zeman, O. Isabella, *Prog. Photovolt. Res. Appl.* **2020**, *28*, 425.

[30] C. Han, Y. Zhao, L. Mazzarella, R. Santbergen, A. Montes, P. Procel, G. Yang, X. Zhang, M. Zeman, O. Isabella, *Sol. Energy Mater. Sol. Cells* **2021**, *227*, 111082.

[31] R. A. Afre, N. Sharma, M. Sharon, M. Sharon, *Rev. Adv. Mater. Sci.* **2018**, *53*, 79.

[32] R. K. Gupta, K. Ghosh, P. K. Kahol, *Appl. Surf. Sci.* **2009**, *255*, 8926.

[33] T. Yamamoto, H. Song, H. Makino, *Phys. Status Solidi C* **2013**, *10*, 603.

[34] L. T. Yan, R. E. I. Schropp, *Thin Solid Films* **2012**, *520*, 2096.

[35] J. Shi, L. Shen, F. Meng, Z. Liu, *Mater. Lett.* **2016**, *182*, 32.

[36] S. Huang, W. Liu, X. Li, Z. Li, Z. Wu, W. Huang, Y. Yang, K. Jiang, J. Shi, L. Zhang, F. Meng, Z. Liu, *Phys. Status Solidi RRL* **2021**, *15*, 1.

[37] Y. Furubayashi, M. Maehara, T. Yamamoto, *J. Phys. D Appl. Phys.* **2020**, *53*, 37510.

[38] Y. Shigesato, S. Takaki, T. Haranoh, *J. Appl. Phys.* **1992**, *71*, 3356.

[39] R. Santbergen, T. Meguro, T. Suezaki, G. Koizumi, K. Yamamoto, M. Zeman, *IEEE J. Photovolt.* **2017**, *7*, 919.

[40] International Electrotechnical Commission, *Photovoltaic Devices: Part 1-2: Measurement of Current-Voltage Characteristics of Bifacial Photovoltaic (PV) Devices*, 1st ed., 27.160 (IEC TS 60904-1-2), VDE Verlag **2019**.

[41] P. Procel, H. Xu, A. Saez, C. Ruiz-Tobon, L. Mazzarella, Y. Zhao, C. Han, G. Yang, M. Zeman, O. Isabella, *Prog. Photovolt. Res. Appl.* **2020**, *28*, 935.

[42] A. Tomasi, F. Sahli, J. P. Seif, L. Fanni, S. M. De Nicolas Agut, J. Geissbuhler, B. Paviet-Salomon, S. Nicolay, L. Barraud, B. Niesen, S. De Wolf, C. Ballif, *IEEE J. Photovolt.* **2016**, *6*, 17.

[43] C. Han, Y. Zhao, L. Mazzarella, R. Santbergen, A. Montes, P. Procel, G. Yang, X. Zhang, M. Zeman, O. Isabella, *Sol. Energy Mater. Sol. Cells* **2021**, *227*, 111082.

[44] G. Limodio, Y. De Groot, G. Van Kuler, L. Mazzarella, Y. Zhao, P. Procel, G. Yang, O. Isabella, M. Zeman, *IEEE J. Photovolt.* **2020**, *10*, 372.

[45] G. Yang, C. Han, P. Procel, Y. Zhao, M. Singh, L. Mazzarella, M. Zeman, O. Isabella, *Prog. Photovolt. Res. Appl.* **2022**, *30*, 141.

[46] Y. Zhao, P. Procel, C. Han, L. Mazzarella, G. Yang, A. Weeber, M. Zeman, O. Isabella, *Sol. Energy Mater. Sol. Cells* **2021**, *219*, 110779.

[47] Y. Zhao, P. Procel, A. Smets, L. Mazzarella, C. Han, G. Yang, L. Cao, Z. Yao, A. Weeber, M. Zeman, *Prog. Photovolt. Res. Appl.* **2023**, *31*, 1170.

[48] C. Han, G. Yang, P. Procel, D. O'Connor, Y. Zhao, A. Gopalakrishnan, X. Zhang, M. Zeman, L. Mazzarella, O. Isabella, *Sol. RRL* **2022**, *6*, 2100810.